#7465

Journal of Wind Engineering and Industrial Aerodynamics, 46 & 47 (1993) 219–228
Elsevier

Computation of Wind Flow around a Tall Building and the Large–Scale Vortex Structure

CHARLES C. S. SONG
Professor
JIANMING HE
Research Associate, *St. Anthony Falls Hydraulic Laboratory, Dept. of Civil and Mineral Engineering, and Minnesota Supercomputer Institute, University of Minnesota, Minneapolis, MN55414, USA*

Abstract

A numerical study of three–dimensional wind flow around a tall building is presented in this paper. The solution is obtained by solving weakly compressible flow equations, along with Smagorinsky's subgrid–scale turbulent model. The numerical scheme is based on MacCormack's predictor–corrector explicit finite volume method. First, the numerical model was verified by testing a shear flow around surface–mounted cube, then a detailed study was carried out for a shear flow around a taller building model (width:length:height = 1:0.889:4.667). The main task of this paper is to explore the large–scale vortex structure and the unsteady behavior of flow around a tall building, which are still not well understood.

1. INTRODUCTION

The flow field around a building consists of a very complicated three–dimensional turbulent vortex structure, which is characterized by stagnation, separation, circulation and unsteadiness. So far, many issues, such as the nature of wake pattern behind the building, the turbulence characteristics in the wake, and the unsteady flow behavior, are far from being fully understood.

For these reasons, wind tunnel testing has been widely used as part of the building design process. The experimental research works on turbulent shear flow over a cube were extensively done by a number of investigators (Castro and Robin, 1977; Peterka and Cermak, 1977; 1986; Okamoto and Uemura, 1991). However, some unsteady flow quantities are so difficult to measure that more reliance on computational approach will occur in future. This trend has been more significant as the rapid development of faster and less expensive supercomputer takes place. In fact, some attempts have been made to find a numerical solution to the Navier–Stokes equations for a full three dimensional flow around a cube. The computed time–averaged pressure and velocity are reported to agree with the experimental data (Paterson and Apelt, 1986; Murakami et al., 1987; Murakami and Mochida, 1988). However, the detailed flow pattern around a cube and the unsteady characteristics have not appeared in the literature. A numerical study of wind flow around a taller building was conducted by Stathopoulos and Baskaran (1990) who attempted to simulate the flow field in half of the flow domain by imposing a symmetrical boundary condition on the plane of symmetry. However, the assumption of flow symmetry precluded the effect of the strong unsteady and non–symmetrical vortex–shedding process from being calculated.

Recently the authors applied weakly compressible flow model with large eddy

simulation approach to the wind flow around a cubical building. The calculated time–averaged velocity field and pressure distribution on the building surfaces agreed well with available experimental data (He and Song, 1992).

A three dimensional numerical modeling of turbulent shear flow around a taller building is presented in this paper. The governing equations, based on weakly compressible flow approach, are used to calculate unsteady flows at small Mach number – large Reynolds number condition (Song and Yuan, 1988). Large scale structures of turbulence are directly calculated, but small–scale turbulence is modeled with a subgrid scale turbulence model. The governing equations are solved numerically using an explicit finite volume method based on MacCormack's predictor–corrector scheme.

2. GOVERNING EQUATIONS

In wind engineering, most flows can be considered to be at low Mach number state, for which the time evolution can be adequately described by a weakly compressible flow model (Song and Yuan, 1988):

$$\frac{\partial p}{\partial t} + K \frac{\partial u_i}{\partial x_j} = 0 \tag{1}$$

$$\frac{\partial u_i}{\partial t} + \frac{\partial}{\partial x_j}(u_j u_i) + \frac{1}{\rho}\frac{\partial p}{\partial x_i} = \nu \frac{\partial^2 u_i}{\partial x_j \partial x_j} \tag{2}$$

where $K=\rho a_0^2$ is the bulk modulus of fluid elasticity, and a_0 is the sound speed.

The pressure time–derivative term in the continuity equation, which is zero in incompressible flow model, is retained to represent the effect of fast acoustic transport.

For turbulent flow, the large eddy simulation approach is adopted. By means of the box filter operation over a small control volume in space (Deardorff, 1970), the momentum equation can be written as:

$$\frac{\partial \bar{u}_i}{\partial t} + \frac{\partial}{\partial x_j}(\bar{u}_j \bar{u}_i) + \frac{1}{\rho_0}\frac{\partial P}{\partial x_i} = \nu \frac{\partial^2 \bar{u}_i}{\partial x_j \partial x_j} - \frac{\partial \tau_{ij}}{\partial x_j} \tag{3}$$

where $P = p + \frac{1}{3}\overline{u_k^2 u_k^2}$ is a modified pressure, and $\tau_{ij} = \overline{u_i^2 u_j^2} - \frac{1}{3}\delta_{ij}\overline{u_i^2 u_j^2}$ is the subgrid scale turbulence shear stress.

The simplest and most widely used subgrid model of the small–scale turbulence is due to Smagorinsky (1963).

$$\tau_{ij} = -\nu_t \left(\frac{\partial \bar{u}_i}{\partial x_j} + \frac{\partial \bar{u}_j}{\partial x_i}\right) \tag{4}$$

and

$$\nu_t = (C_s \Delta)^2 (\bar{S}_{ij}\bar{S}_{ij})^{1/2} \tag{5}$$

where C_s is a model coefficient, $\bar{S}_{ij} = \frac{\partial \bar{u}_i}{\partial x_j} + \frac{\partial \bar{u}_j}{\partial x_i}$, and Δ is a length associated with the filter. For brevity, the bar will be dropped out in the following expressions.

The governing equations are solved numerically using the well–known explicit finite volume method based on MacCormack's predictor–corrector scheme (MacCormack, 1969).

To avoid the necessity of using extremely small grids near solid wall, a wall function, or a partial slip condition, is applied (Yuan et al., 1991). The log law is assumed to hold near the wall for the time averaged velocity:

$$\overline{u} = 2.5\ \overline{u}^*\ \ln\ |\ 9.0\ \overline{u}^*\ y/\nu\ | \tag{6}$$

where $\overline{u}^* = \text{sign}(\overline{\tau}_w)(|\overline{\tau}_w|/\rho)^{1/2}$ is the time averaged wall shear velocity, $\overline{\tau}_w$ is the wall shear stress, and the bar here represents a time–averaged value.

At upstream, the velocity profile can be given using desired condition. In the field of wind engineering, a power law $u/u_0=(y/\delta)^{\alpha}$ is assumed in the boundary layer, where α=1/4 in urban area with large roughness and 1/7 in rural area with small roughness. In addition, the following conditions are also specified at the upstream end,

$$v = w = 0,\ \frac{\partial P}{\partial x} = 0 \tag{7}$$

At far downstream, it is assumed that

$$\frac{\partial u}{\partial x} = \frac{\partial v}{\partial x} = \frac{\partial u}{\partial x} = \frac{\partial P}{\partial x} = 0 \tag{8}$$

3. MODEL VALIDATION

The method described above was first applied to the case of flow around a surface–mounted cube (He and Song, 1992). Two grid systems (67x27x43 and 75x31x51) were tested in this case. The fine mesh 75x31x51 was obtained by inserting additional grids in the region near the front edges where extremely large velocity and pressure gradients exist.

The unsteady flow field in this case is very complex, but there appears to be a coherent structure consisting of four major vortex systems. They are, 1) the secondary currents generated by the flow separation on the roof and the large circulation cavity behind the building having axes in the width wise direction, 2) the Karman vortex street with axes in the vertical direction, 3) the horseshoe vortex around the building near the ground, and 4) the twin axial vortices issuing from the side edges of the roof. More detailed description of the large scale vortex structure will be given later.

He and Song (1992) compared the calculated time–averaged pressure coefficient with the available experimental data reported by Castro and Robins (1977) along two center lines on the surface of the cube, as shown in Fig. 1. It was found that the calculated results with fine mesh system agreed well with the experimental data but the coarse mesh system produced some errors near the edges of the cube. Comparison between predicted and measured (Castro and Robins, 1977) profiles of mean velocity defect is shown in Fig. 2. Fig. 2(a) shows the horizontal profiles of velocity defect at half body height. The velocity defect ΔU is defined as:

$$\Delta U = \frac{u_1(z)-u(z)}{u(\delta)} \tag{9}$$

where $u(z)$ is the longitudinal velocity component, $u_1(z)$ is the corresponding value without building (input profile), and $u(\delta)$ is the reference velocity. The numbers shown on the top axis represent the x/h coordinates of the sections where ΔU are plotted.

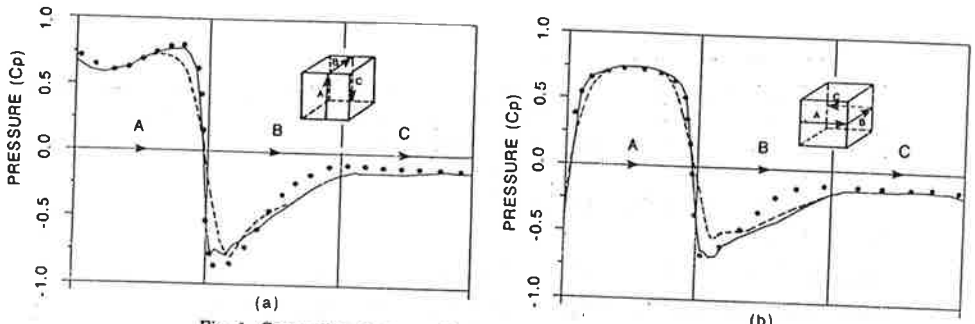

Fig. 1 Comparison between the computed and measured mean pressure coefficient distribution on a cubical obstacle; • measured data (Castro and Robins, 1977); dash line: computed values with coarse mesh (67x27x43); solid line: computed values with fine mesh (75x31x51).

The number on the bottom axis represents the scale of the velocity defect. Fig. 2(b) is the vertical profiles of the similar velocity defect on the plane of symmetry. It is shown that the predicted results are generally in good agreement with experimental data.

An interesting flow feature is the over correction of velocity defect causing negative velocity defect in the far wake region. It begins at the section of 9 building height (h) downstream, and becomes more apparent further downstream. This flow feature was also found in previous experiments by Peterka and Cermak (1977), and Kotheri et al. (1986). Reportedly the vortices persist up to 80h downstream of the obstacle. Its existence is known to be accompanied with a pair of axial vortices as shown in Fig. 3, where the secondary velocity and the corresponding vorticity contour at the downstream section are displayed. The vortices near the ground in Fig. 3(b) is induced by the outward boundary layer flow. A number of authors (Castro and Robin, 1977; Peterka and Cermak, 1977; Kotheri et al., 1985) believed that the axial vortices are extension of the horseshoe vortices which transfer higher momentum fluid from the top of the boundary layer into the wake. However, by comparing the detailed velocity fields around the cubic building and that of a taller building which will be described later, the authors are convinced that the axial vortices are mainly due to the downwash of the main stream from above toward the wake region.

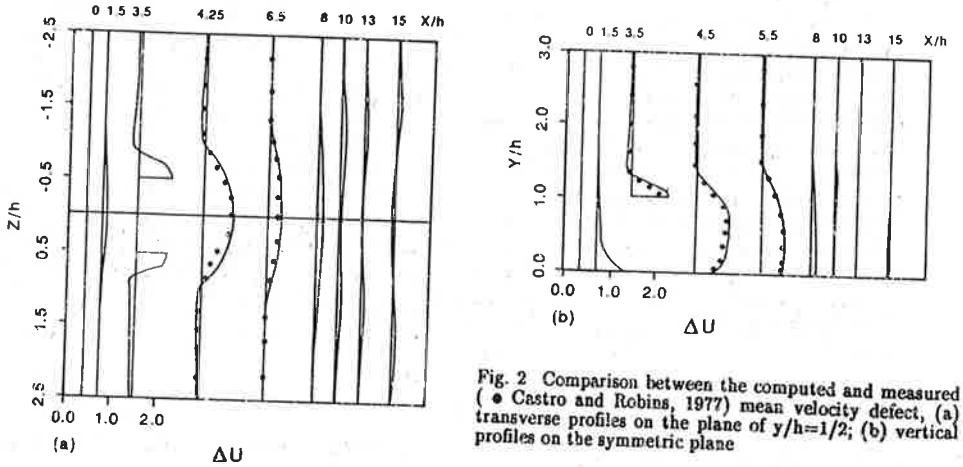

Fig. 2 Comparison between the computed and measured (• Castro and Robins, 1977) mean velocity defect, (a) transverse profiles on the plane of y/h=1/2; (b) vertical profiles on the symmetric plane

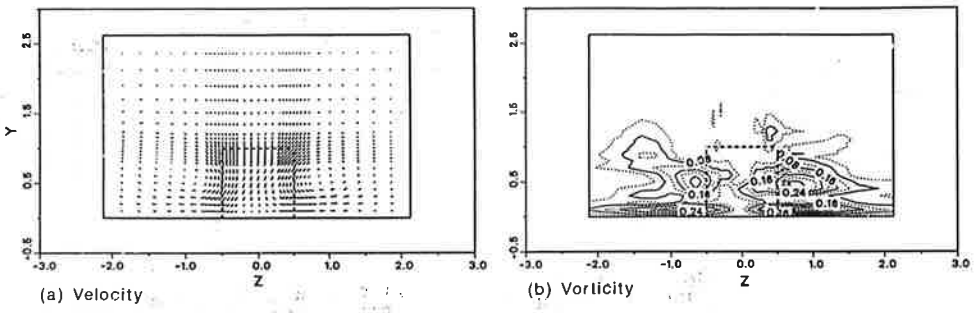

Fig. 3 Computed time–averaged secondary current (a) and vorticity contour (b) of the flow around a cubical building at the downstream section, x/D=15

4. TALL BUILDING CASE

4.1 Problem Definition

Computationally, there is no significant difference between a flow around a cube and a tall building. However, from practical point of view, flow around a tall building is more important in engineering applications. In fact, the model which is studied here is a simplified version of a real building.

Physically, flow around a tall bluff body also generates a quite different flow structure from that around a cube. It will be found that the flow information around a tall body is very useful to the understanding of the physical nature of the vortex structure around a bluff body.

As stated before, one of the advantages of this numerical model is its ability to simulate the unsteady process. In this section, a numerical study on a turbulent shear flow around a tall building with width(D):length:height = 1.0:0.8889:4.6667 is presented. The main effort of this study is to concentrate on the understanding of the flow pattern and the particular characteristics related to increased building height. By comparing the results with those in the flow around a cube, better understanding of the turbulent vortex structure of flow around a bluff body is expected.

A mesh system of 61x39x39 is used considering the fact that in three dimensional flow the mesh refinement does not significantly affect the flow features for this study and many engineering applications. The building is divided into 8 uniform segments in flow direction, 10 uniform segments in transverse direction, and 25 non–uniform segments in vertical direction. To simulate a weather condition close to ocean, 1/7 power law is assumed as the input profile.

4.2 Time–Averaged Vortex Structure

The velocity fields at two levels are shown in Fig. 4. On the plane close to the ground, as shown in Fig. 4(a), the reverse flow induced by the horseshoe vortex at the front side is noticeable. At the section close to the roof, as shown in Fig. 4(b), the intensity of the symmetric vortex in the cavity behind the building is very large. This is apparently due to the combination of the Karman vortex and the shed vortex from the roof that tend to reinforce each other.

The time–averaged velocity and vorticity fields on the vertical plane of symmetry are shown in Fig. 5. The vortex generated by the flow separation at the leading edge of the roof (A) and the horseshoe vertex near the ground of the front (B) can be clearly seen in Fig. 5(b).

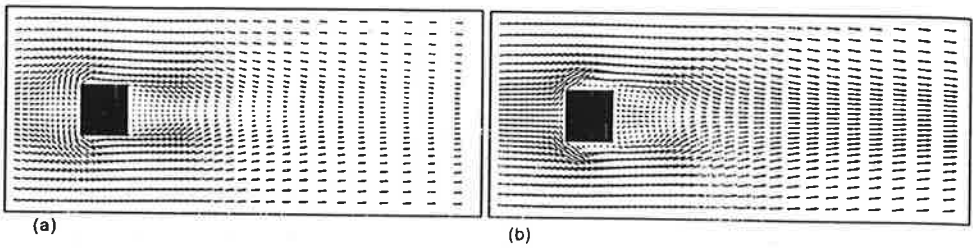

Fig. 4 Computed time–averaged velocity fields on horizontal planes at two different levels in a shear flow around a tall building, (a) close to the ground; (b) close to the roof

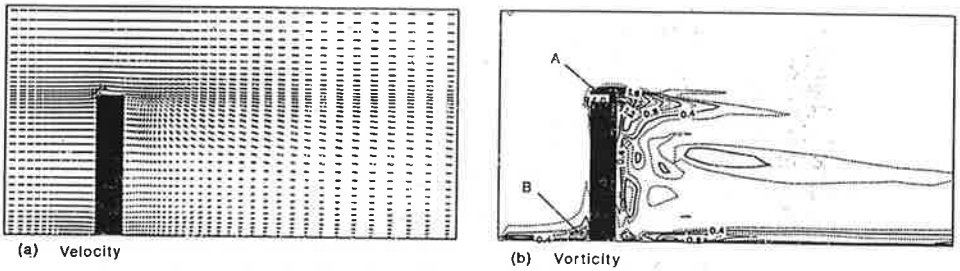

Fig. 5 Computed time–averaged velocity and vorticity component contour on the symmetrical plane in a shear flow around a tall building

The velocity and vorticity fields at four cross–sections normal to the main flow direction are shown in Fig. 6. At the middle section of the building (X=x/D=3.4), as shown in Fig. 6(a), three different vortices: the tip vortices generated at the two side corners, the horseshoe vortices inclined from the building front, and the boundary vortices produced by outward flow are indicated by C, B and F, respectively. At one building width downstream from the building (X=4.8), as shown in Fig. 6(b), more complicated vortex structure is displayed. The tip vertices are much strengthened and pushed downward by the downwash of the main stream from above, as indicated by C. The velocity vectors show that the wake recovery at low level section is faster than that in the middle section. The non–uniform wake recovery on the cross–section also induces a pair of large vortices, as denoted by D. As a by–product, the vortices also generates the inward boundary vortices, indicated by E. At the same time, due to the strong wake recovery, the outward boundary vortices (F) are largely demolished, and the horseshoe vertices (B) are also much weakened. At about two building width downstream from the building (X=6.0) in Fig. 6(c), vortices B and F completely disappeared. At the far downstream section (X=15) in Fig. 6(d), vortices C dominate the wake but its counter part is very much weaker while the other vortices nearly disappeared. From these figures, it is very clear that the twin opposite vortices (C) in the far wake region originate from the building top side corners, and are strengthened by the strong downwash of main stream. Again, they are not related to the horseshoe vortices. In fact, the horseshoe vortices are completely destroyed by the strong wake recovery in the cavity region. The unsteady vortex–shedding may be another factor resulting in the horseshoe vortex destruction in the cavity region.

In order to further trace the horseshoe vortex, the vorticity component ω_x is now

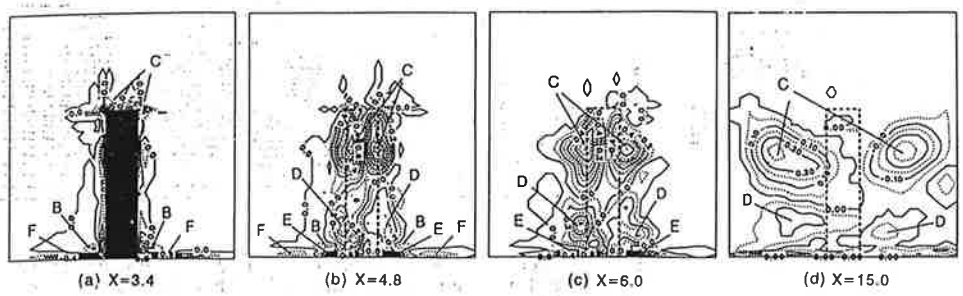

Fig. 6 Computed time–averaged vorticity component contours (ω_x) at 4 cross–sections in a shear flow around a tall building

plotted on a horizontal plane, passing through the center of the horseshoe vortices (Fig. 7a) and a side–view vertical plane very close to a building side (Fig. 7b). Fig. 7(a) clearly shows that the horseshoe vortices (B) diffuse outward and gradually weaken until disappearing at about two building width downstream. The vortices induced by the non–uniform wake recovery (D) start from the cavity close to the center line. The horseshoe vortex can also be seen near the side corner in Fig. 7(b). Apparently, there is no relation between the horseshoe vortex (B) and the twin vortices (A). These figures most clearly show that the twin vortices C originate near the building top side edges, then are strengthened and swept downward by the main stream downwash in the cavity region, and finally extend far downstream.

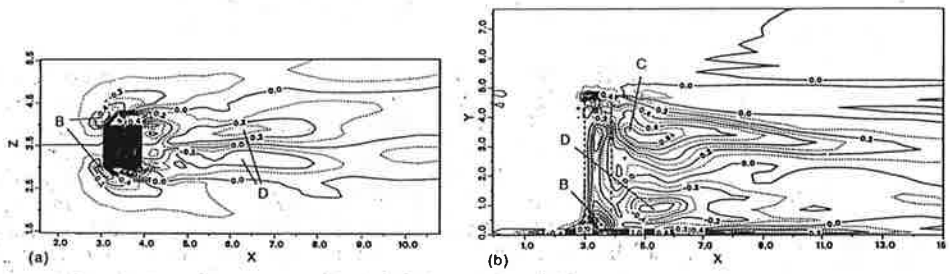

Fig. 7 Computed time–averaged vorticity component contours (ω_x) on near ground plane (a) and a vertical plane close to building side (b) in a shear flow around a tall building

4.3 Unsteady Characteristics

As revealed by the time–averaged velocity and vorticity fields just described, there are several different types of large–scale vortices combined to produce a very complex flow field. Moreover, these large–scale vortices are all time dependent to some degree making the time–averaged picture somewhat misleading. Detailed analysis of the calculated instantaneous values reveals, however, that the dominant mechanism of flow unsteadiness of the large–scale structure is the Karman vortex shedding. The flow pattern on the horizontal plane through the half height of the building is very much like that of the flow around a two–dimensional cylinder. But the period of oscillation is somewhat longer and less regular due to the three–dimensional effect. Fig. 8 shows a series of velocity fields at half building height plane during one period of the vortex shedding.

One evidence of the strong dependence of the flow on Karman vortex shedding can be seen from the plot of drag and lift coefficients as functions of time, as shown in Fig. 9. The values shown in Fig. 9(a) are for the entire building but those of Fig. 9(b) are the values at the half building height. Note that the lift and drag coefficients oscillate at larger amplitude at the midsection than for the entire building.

Fig. 10(a) and 10(b) show one instantaneous velocity field and corresponding vorticity component on the plane of symmetry, respectively. Compared with the time–averaged results in Fig. 5, the instantaneous flow pattern on the plane is much more complicated due to the strong interaction of the unsteady three–dimensional vortices in the wake. It is also very difficult to observe the time variation of the flow pattern without using numerical visualization technique.

Two instantaneous velocity vector fields on a cross–section at X=15 shown in Fig. 11 illustrate the time dependence of the twin vortices designated by C in Figs. 5 and 6. Both the intensity and location of these vortices change more or less periodically in lateral direction. It is worth noting that the height of the vortices increases with the building height. This result again excludes the argument that the axial twin vortices are an extension of the horseshoe vortices, as stated before.

5. CONCLUSIONS

The prediction of three dimensional shear flow around a surface–mounted cube agrees very well with previous experimental data. The large–scale vortex structure of the turbulent shear flow around a tall building is analyzed based on the current

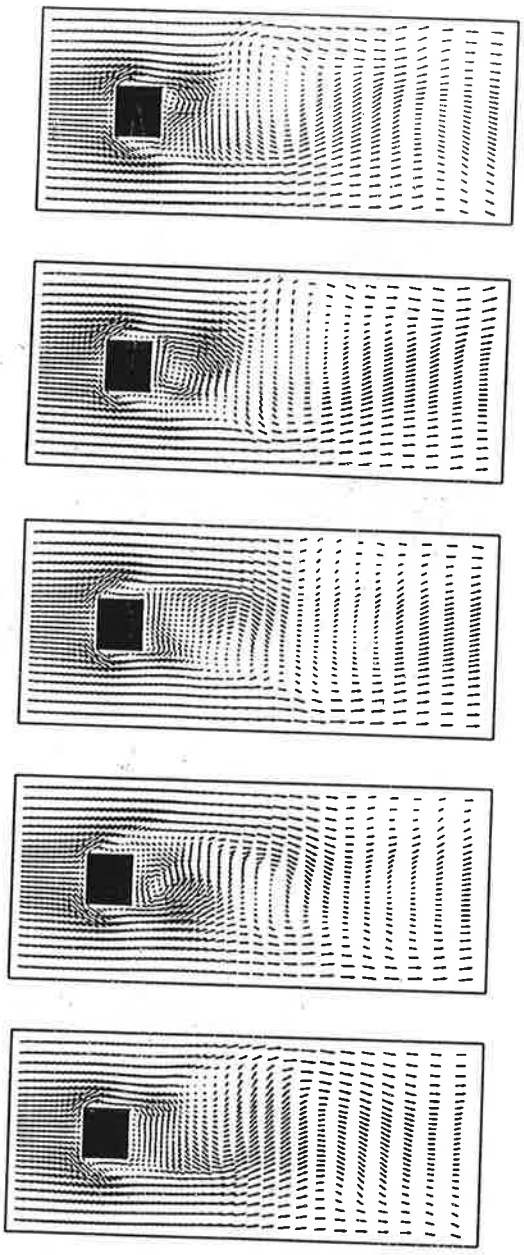

Fig. 8 A series of instantaneous velocity vectors in a shear flow around a tall building at half body height during one period of vortex–shedding process

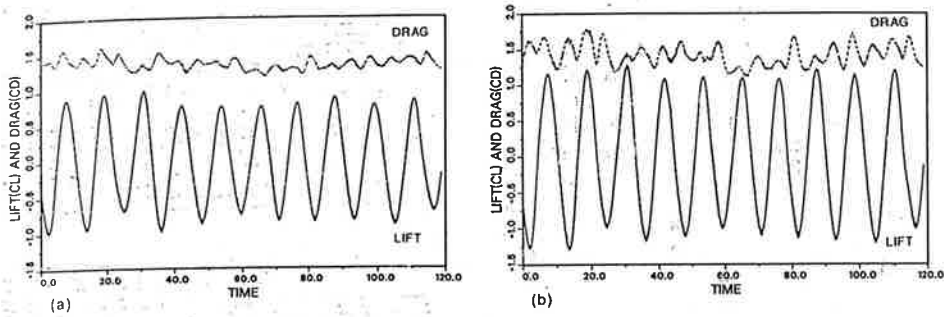

Fig. 9 The lift and drag coefficient (C_l and C_d) fluctuations in a shear flow around a tall building; (a) over entire building surfaces; (b) at half building height, per unit length

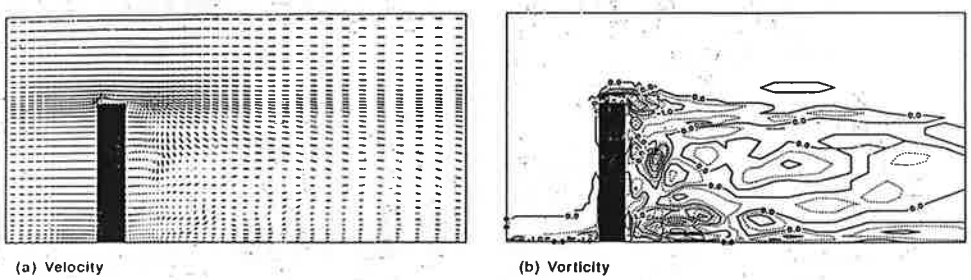

Fig. 10 One instantaneous velocity and vorticity field on the symmetrical plane in a shear flow around a tall building

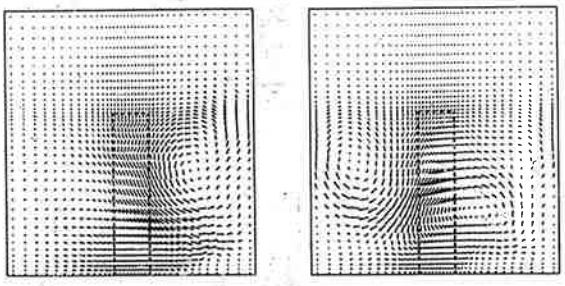

Fig. 11 Two instantaneous velocity fields at the downstream section (x/D=15) in a shear flow around a tall building

computation.

The computed results show that the twin axial vortices have no relation with the horseshoe vortex even though both kinds of vortices have similar flow pattern viewed over a cross–section. It is found that the twin axial vortices are first produced by the roof side edges, like tip vortex, then strengthened by the downwash from main stream.

Unsteady vortex–shedding is also found on the vertical plane of symmetry. The unsteadiness is induced by Karman vortex–shedding. Therefore, the frequency of the roof vortex–shedding is twice as large as that of Karman vortex shedding. Karman vortex–shedding also induces lateral oscillation of the twin opposite vortices on the cross–section.

ACKNOWLEDGEMENTS

This research was sponsored by The 1991–1992 Cray Research University Grant Program, the Minnesota Supercomputer Institute and the Minnesota Supercomputer Center of the University of Minnesota, and the Legislative Commission on the Minnesota Resources. The second author would like to recognize the support of the 1992–1993 Minnesota Supercomputer Institute research scholarship.

REFERENCES

Castro, I. P. and Robins, A. G., 1977, "The flow around a surface–mounted cube in uniform and turbulent streams," *J. Fluid Mechanics*, Vol. 79, pp. 307–335.

Deardorff, J. W., 1970, "A numerical study of three–dimensional channel flow of large Reynolds numbers," *J. Fluid Mechanics*, Vol. 41, Part 2, pp. 453–480.

He, J., and Song, C. C. S., 1992, "Computation of turbulent shear flow over a surface–mounted obstacle with large eddy simulation," *Journal of Engineering Mechanics, ASCE*, Vol. 118, No. 11, pp. 2282–2297.

Kotheri, K. M., Peterka, J. A. and Meronney, R. N., 1986, "Perturbation analysis and measurements of building wakes in a stably stratified turbulent boundary layer," *J. Wind Eng. Ind. Aerdyn.*, Vol. 25, pp. 49–74.

MacCormack, R. W., 1969, "The effect of viscosity in hypervelocity impact cratering," *AIAA Paper* No. 69–354.

Murakami, S. and Mochida, A., 1988, "3–D numerical simulation of airflow around a cubic model by means of the κ–ϵ model," *J. Wind Eng. Ind. Aerdyn.*, Vol. 31, pp. 283–303.

Murakami, S. Mochida, A., and Hibi, K., 1987, "Three–dimensional numerical simulation of airflow around a cubic model by means of large eddy simulation," *J. Wind Eng. Ind. Aerdyn.*, vol. 25, 291–305.

Okamoto, S., and Uemura, N., 1991, "Effect of rounding side–scorers on aerodynamic forces and turbulent wake of a cube placed on a ground plane," *Experiments in Fluids*, Vol. 11, pp. 58–64

Paterson, D. A and Apelt, C. J., 1986, "Computation of wind flows over three–dimensional buildings," *J. Wind Eng. Ind. Aerdyn.*, Vol. 24, pp. 192–213.

Peterka, J. A. and Cermak, J. E., 1977, "Turbulence in building wakes," *4th Int. Conf. on Wind Effects on Buildings and Structures*, Heathrow, England, Cambridge Univ. Press, London.

Smagorinsky, J., 1963, "General circulation experiments with primitive equations," *Month Weather Review*, Vol. 91, No. 3, pp. 99–164.

Song, C. C. S., and Yuan, M., 1988," A weakly compressible flow model and rapid convergence methods," *Journal of Fluids Engineering*, Vol. 110, pp. 441–445.

Stathopoulos, T., and Baskaran, A., 1990, "Boundary treatment for the computation of three–dimensional wind flow conditions around a building," *J. Wind Eng. Ind. Aerdyn.*, Vol. 35, pp. 177–200.

Yuan, M., Song, C. C. S, and He, J., 1991, "Numerical analysis of turbulent flow in a two–dimensional nonsymmetric plane–wall diffuser," *Journal of Fluids Engineering*, Vol. 113, pp. 210–215.